DIAMOND

Chameleon, with Nickel Absorption Band

The Carlsbad laboratory recently examined a 0.31 ct Light greenish yellow marquise-cut diamond. The stone displayed the strong yellow fluorescence, persistent yellow phosphorescence, and green color component of a chameleon diamond. A chameleon diamond has a green or greenish color component under normal conditions. When heated or left in the dark for long periods of time, the green component temporarily disappears, giving way to an orange component. Figure 1 shows the diamond before and immediately after heating, in which the removal of the green component leads to an orange-dominant hue, demonstrating that the stone was in fact a chameleon diamond. Unfortunately, the stone's low saturation makes the effect less noticeable.

Examination of the visible-NIR spectrum revealed a noticeable nickel-related absorption band at 685 nm (figure 2). DiamondView images were taken to prove the stone was not synthetic, as nickel is a common catalyst in HPHT synthetics (figure 3). While nickel has long been known to occur as a trace element in chameleon diamonds (T. Hainschwang et al., "A gemological study of a collection of chameleon diamonds," Spring 2005 *G&G*, pp. 20–34), its role in the color-change effect is unknown. Nickel has also been reported as a cause of green coloration in certain diamonds (W. Wang et al., "Natural type Ia diamond with green-yellow color due to Ni-related de-

Figure 1. The chameleon diamond is shown before and after heating (left and right).

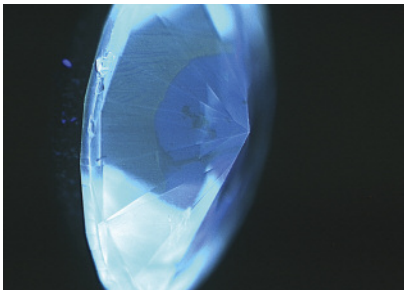

Figure 3. DiamondView imaging showed uneven blue and green fluorescent zones, proving the stone's natural origin.

Figure 2. The absorption spectrum of the chameleon diamond shows a nickel-related band at 685 nm.

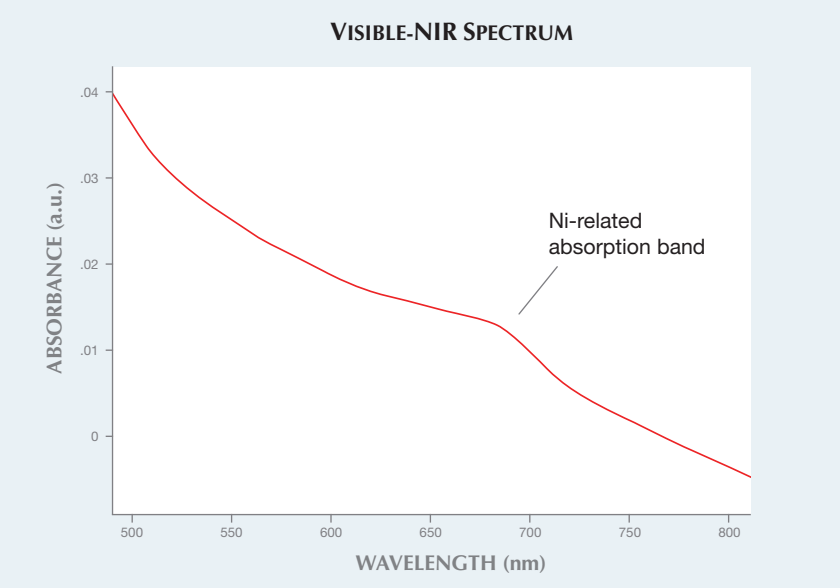

Editors' note: All items were written by staff members of GIA laboratories.

GEMS & GEMOLOGY, Vol. 50, No. 2, pp. 151–157, http://dx.doi.org/10.5741/GEMS.50.2.151.

© 2014 Gemological Institute of America

fects," Fall 2007 *G&G*, pp. 240–243), but this may be the first time it has been identified as the major cause of a green component in a chameleon. The rarity of chameleon diamond, combined with the rarity of Ni-related natural green diamonds, makes this a truly unique specimen.

Troy Ardon

Long-Term Durability of CVD Synthetic Film on Natural Diamond

In 2005, a thin film (< 10 µm) of synthetic diamond grown by chemical vapor deposition was deposited on the pavilion of a 0.27 ct natural diamond. The CVD layer was deliberately doped with boron to create a bluish color. No subsequent polishing was performed. Rather than blue, the resulting color was a less desirable gray. This natural diamond with CVD overgrowth was then reset in a ring and worn daily by the author for the next eight years. Recently, this hybrid diamond was removed from its setting for gemological and spectroscopic characterization and to assess the current state of the CVD film.

Well-controlled durability studies have examined non-diamond coatings on diamond (e.g., A.H. Shen et al., "Serenity coated colored diamonds: Detection and durability," Spring 2007 *G&G*, pp. 16–34) and nanocrystalline diamond coatings on non-diamond materials (J.E. Shigley et al., "Characterization of colorless coated cubic zirconia [Diamantine]," Spring 2012 *G&G*, pp. 18–30). To our knowledge, however, none have been performed on CVD diamond films grown on natural diamond. The assessment of this one sample, given the exposure a ring is usually subjected to, can indicate the long-term stability of such coatings on diamond. The expectation was that such films would remain stable, as there is no lattice mismatch in the crystal structure between the CVD synthetic film and the natural diamond. Lattice mismatch and the resulting low cohesion at the diamond/non-diamond interface typically result in moderate to very poor durability.

It was difficult to find evidence of the CVD layer using spectroscopic techniques. FTIR absorption (which generally provides data from the bulk of the diamond) revealed no CVD-specific features, only that the underlying diamond was type Ia. Using PL spectroscopy, which collects data from a limited area, it was difficult to find spectroscopic evidence of the CVD film, even when the PL data were collected in confocal mode. No CVD-related 3123 cm^{-1} peak was detected in IR absorption, and the silicon peak at 737 nm was not observed in PL. The best evidence of the CVD layer's continued existence on the diamond was from its unusual appearance in visual observation (figure 4) and microscopic analysis (figure 5). The pavilion also showed electrical conductivity, which provides another indication of the boron doping.

By examining the pavilion of the diamond at high magnification, we could assess the condition of the CVD layer after eight years of daily wear. The film was still largely intact, covering the entire pavilion and containing only a few sporadic pinholes. There was no noticeable degradation at the facet junctions. The obvious color zoning in figure 4 that appears to divide the diamond into quadrants

Figure 4. This 0.27 ct diamond with a boron-doped CVD synthetic diamond film on the pavilion received a color grade of Fancy Dark brownish yellowish gray. The distinct color zoning seen in this photo makes it apparent that the diamond has been treated in some way and is not a natural stone.

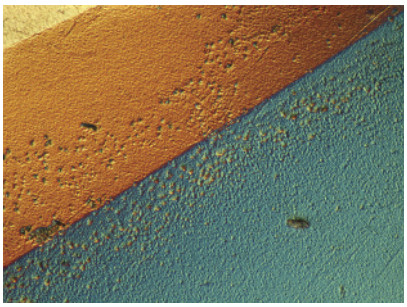

Figure 5. This differential interference contrast image shows the irregular texture of the CVD overgrowth film on the pavilion facets of the 0.27 ct natural diamond. Each facet is a different color, and the boundaries between colors are facet junctions. Field of view 246 microns.

is likely due to differences in deposition and boron incorporation rates on the various facets. Recently, the diamond was annealed twice, at 600°C and 700°C for one hour each in a reducing atmosphere, in an effort to make it appear bluer. This treatment changed the color from Fancy Dark brownish yellowish gray to Fancy Dark gray.

As treatments become more sophisticated and move from the laboratory into the trade, the need for accurate detection only intensifies. Nevertheless, such semipermanent films are identifiable and reiterate the need to use both spectroscopic and traditional methods for gemological characterization.

Sally Eaton-Magaña

Star OPAL

Opal is best known for displaying play-of-color. It may also display asterism, though star opal has only been reported from Idaho, and a perfect six-rayed star is exceptionally rare (J.V. Sanders, "The structure of star opals," *Acta Crystallographica*, Vol. A32, 1976, pp. 334–338). The Bangkok laboratory recently had the opportunity to examine a transparent star opal (figure 6). The 2.39 ct light brownish yellow cabochon displayed a distinct six-rayed star.

Standard gemological testing gave a spot RI reading of 1.43 and a hydro-

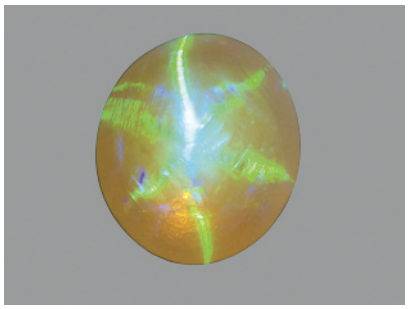

Figure 6. This 2.39 ct transparent opal with a light brownish yellow bodycolor possessed a six-rayed star.

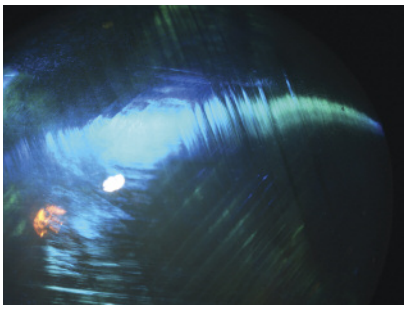

Figure 7. This photomicrograph of the opal shows the intersection of large parallel planes with play-of-color, producing asterism. Magnified 15×.

static SG of 2.10. When exposed to ultraviolet radiation, the stone fluoresced strong bluish white under long-wave and weak bluish white under short-wave UV. It phosphoresced green after exposure to long-wave UV. Advanced gemological testing by energy-dispersive X-ray fluorescence (EDXRF) confirmed a silica-rich material with some additional trace elements, including aluminum and iron. All of these properties were consistent with opal.

Microscopic examination revealed large parallel planes with play-of-color intersecting to form a hexagonal pattern (figure 7). This is responsible for producing the six-rayed star. This unusual stone serves as a reminder that, unlike asterism in other gem materials, the star in opal is caused by diffraction of light from faults or imperfections in the packing arrangement of silica spheres.

Wasura Soonthorntantikul

Shell PEARL as a Pearl Imitation

Imitation pearls made of shell, or "shell pearls," have a long history in the jewelry market and have been reported in previous Lab Notes columns (Fall 1984, p. 170; Winter 1986, p. 239; Summer 2001, pp. 135–136; Summer 2004, p. 178). The shell beads are often coated with artificial materials to simulate a wide variety of natural and cultured pearls in the market. Recent submissions of such imitations to GIA prompted researchers in the lab to obtain several samples from a commercial website. Labeled as shell pearls (figure 8), they resembled Tahitian black, white, and yellow/golden South Sea cultured pearls.

Although the samples were similar in appearance and heft to cultured pearls, routine gemological tests revealed unnatural surface characteristics. The black shell pearl necklace also exhibited multicolored but rather oily orient. Magnification showed numerous minute particles with a glittering effect (figure 9, top), as well as a lack of the obvious overlapping nacre platelets commonly found in nacreous pearls. These features suggested that an artificial coating had been applied to the bead. Inspection

Figure 8. These shell pearls range from 10 to 12 mm and display black, white, and golden colors.

Figure 9. Top: The surface of the imitation pearls contained a glittery coating rather than overlapping nacre platelet structures (magnified 112.5×). Bottom: White bead-like shell material was exposed at a damaged area near the drill hole (magnified 10×).

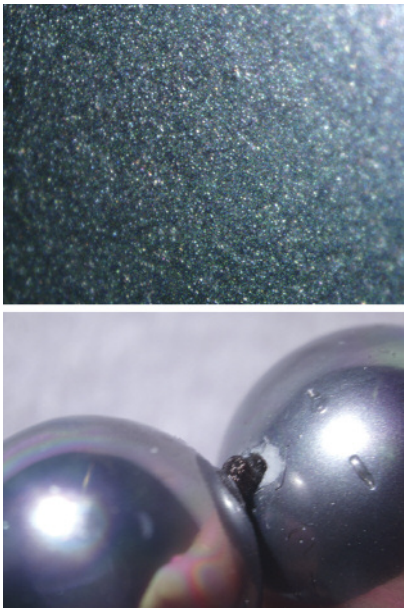

near the drill holes of some samples revealed chipping and peeling of this very thin coating, exposing white bead-like shell material underneath (figure 9, bottom).

X-radiography showed only the inner bead, with occasional parallel banding and cracks—similar to the banding and trematode "tunnels" common in some saltwater shell beads—while the outer coating remained transparent (figure 10). EDXRF analysis detected a high concentration of bismuth, which usually does not occur in pearls but had been reported previously in coated natural and cultured pearls (Fall 2005 Gem News International, pp. 272–273; Winter 2011 Lab Notes, pp. 313–314). Finally, Raman spectroscopic analysis of the exposed white bead identified it as aragonite. These results, coupled with the bead's inert reaction under X-ray fluorescence, confirmed it was made of saltwater shell.

We have noted the use of the terms *shell pearl* or just *pearl* for such imitations in product descriptions on numerous commercial websites. Such inappropriate nomenclature could be misleading to inexperienced buyers. According to the CIBJO Blue Book on pearls, "Imitations or simulants of natural pearls and cultured pearls … shall be immediately preceded by the word 'imitation' or 'simulated', with equal emphasis and prominence . . . as those of the name itself." *Imitation pearl* would be the proper name of this material, and consumers need to be aware of its true identity.

Jessie (Yixin) Zhou and Chunhui Zhou

Figure 10. X-radiography revealed banding and cracks in the inner shell beads.

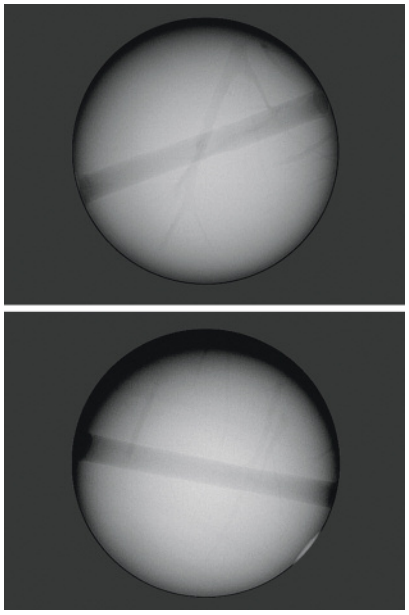

Figure 11. This 0.40 ct square-shaped type Ib CVD synthetic diamond was color graded as Fancy yellow.

Yellow CVD SYNTHETIC DIAMOND

Gem-quality CVD-grown synthetic diamonds are usually type IIa and occasionally type IaA. In addition, a faceted type Ib yellow CVD synthetic of 3 mm in diameter was reported more than a decade ago (J.E. Butler, "Chemical vapor deposited diamond: Maturity and diversity," *Interface*, Spring 2003, pp. 22–26). To the best of our knowledge, no other type Ib examples have been documented in the gem industry since then. The New York laboratory recently examined a gem-quality type Ib CVD-grown synthetic diamond. This Fancy yellow square weighed 0.40 ct and measured 4.20 × 4.12 × 2.55 mm (figure 11).

As is typical for CVD synthetics, the strong silicon-vacancy ($[Si\text{-}V]^-$) center was detected as a doublet at 736.5 and 736.9 nm in the 633 nm PL spectrum. The mid-IR spectrum showed a single substitutional nitrogen atom (N_s^0) at 1130 and 1344 cm^{-1} (figure 12). The nitrogen content, which contributed to the yellow color, was calculated from absorption bands in the

Figure 12. The yellow CVD synthetic's mid-IR spectrum revealed single substitutional nitrogen atoms (N_s^0) at 1130 and 1344 cm^{-1}. The diamond Raman band was detected at 1331 cm^{-1}. A hydrogen-related defect was detected at 3107 cm^{-1}, and C-H defects could be observed at 2948, 2920, 2905, 2873, and 2849 cm^{-1}. An unknown doublet was also observed at 3030 and 3032 cm^{-1}.

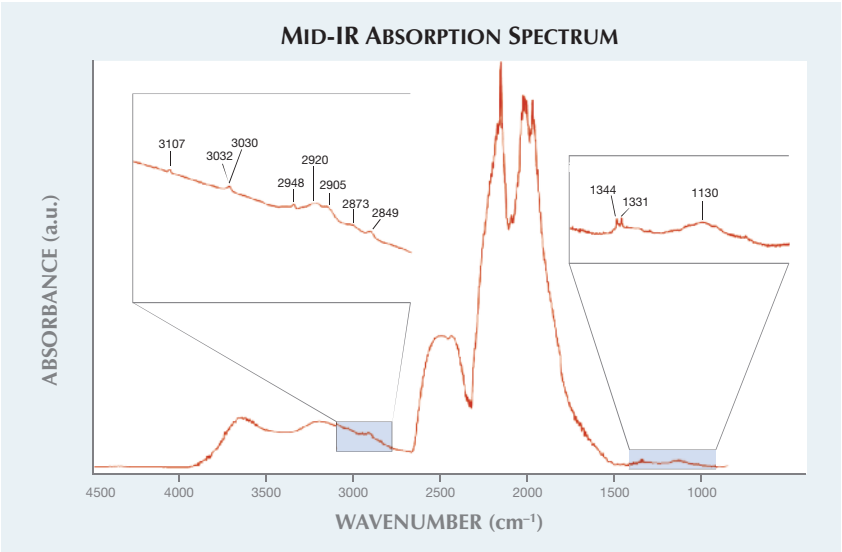

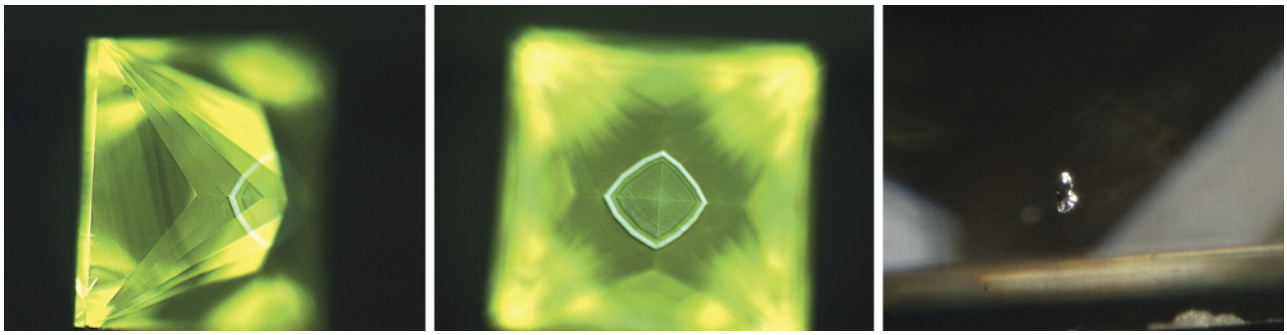

Figure 13. DiamondView imaging revealed curved green lines, reflecting changes in growth conditions (left). Pronounced growth events were also observed in green and bluish green regions near the culet (middle). Microscopic examination revealed a graphitized stress halo (right, magnified 112.5×), along with small feathers on the girdle (not shown).

1000–1400 cm^{-1} mid-IR spectral region as 4.5 ppm. Nitrogen can be unintentionally introduced during the growth process; it can also be added deliberately to control the growth rate of single-crystal CVD synthetic diamond. DiamondView images showed curved green lines, indicating changes in conditions during growth (figure 13, left). The DiamondView also revealed green and greenish blue regions of pronounced growth events near the culet, as in the middle image of figure 13. A graphitized stress halo (figure 13, right) and small feathers on the girdle were observed under the microscope. Typical CVD strain—a localized tatami-like structure with low-strain interference colors—was visible under cross-polarized light.

Post-growth treatment was detected: a hydrogen-related defect at 3107 cm^{-1} and C-H defects at 2948, 2920, 2905, 2873, and 2849 cm^{-1} (again, see figure 12). We did not observe the neutral charge state of the nitrogen vacancy–hydrogen complex ($[N\text{-}V\text{-}H]^0$) at 3123 cm^{-1}. These results suggested that the sample was HPHT-treated. An unknown doublet at 3030–3032 cm^{-1} was also found. Strong N-V (nitrogen-vacancy) defects at 575 (NV^0) and 637 (NV^-) nm were detected in PL spectrum using a 514 nm laser. The negatively charged nitrogen vacancy–hydrogen complex ($[N\text{-}V\text{-}H]^-$) is usually contained in as-grown nitrogen-doped single-crystal CVD synthetic diamond, but it is unstable. After HPHT treatment, the hydrogen atoms were dissociated, causing C-H and N-V defects to form. Additional defects, such as H3 and H2, were also detected. Both centers could be introduced in as-grown CVD synthetic diamonds by HPHT annealing. The H3 centers were responsible for the observed green dislocations in the DiamondView image. As-grown CVD synthetic diamonds usually possess an unattractive brown color component. This can be removed by HPHT treatment to achieve an attractive yellow color, as observed in this sample.

Type Ib CVD synthetics are also of interest for technological applications, especially for quantum computing (see E. Gibney, "Flawed to perfection: Ultra-pure synthetic diamonds offer advances in fields from quantum computing to cancer diagnostics," *Nature*, Vol. 505, 2014, pp. 472–474). The N-V electron spin could be used as a basic unit of quantum computing, known as a quantum bit or "qubit." Qubits are not limited to the binary "0" or "1" states of bits in traditional computers, but can simultaneously exist in both binary states and any state in between—a difficult concept to grasp but one that will lead to vastly enhanced computational capacity. Type Ib yellow CVD diamonds of micrometer size were grown and subsequently electron beam–irradiated and annealed by P. Neumann to create NV centers, as noted in his 2012 PhD thesis, "Towards a room temperature solid state quantum processor: The nitrogen-vacancy center in diamond." After irradiation, the color changed from the as-grown yellow to green, then to purplish pink after annealing.

Kyaw Soe Moe, Wuyi Wang, and Ulrika D'Haenens-Johansson

Flux-Grown SYNTHETIC RUBY with Hydrothermal Synthetic Seed Crystal

The Carlsbad laboratory recently received a 1.18 ct transparent red octagonal step-cut stone for ruby report service. Standard gemological testing established the following properties: RI—1.762 to 1.770; birefringence—0.008; optic sign—uniaxial negative; pleochroism—orangy red to purplish red; specific gravity—4.01; fluorescence reaction—strong red to long-wave, weak red to short-wave UV radiation. Examination with a desk-model spectroscope revealed a typical ruby spectrum. All of these properties were consistent with natural or synthetic ruby.

Under magnification, the most distinctive internal characteristic in the crown was the presence of strong irregular growth features: zigzag- or mosaic-like striated patterns (figure 14), typical of a hydrothermal synthetic. Other areas of the ruby lacking these irregular growth features contained hexagonal metallic platelets and high-relief, whitish flux inclusions (figure 15), typical of a flux-grown synthetic. Flux and hydrothermal inclusions have not been previously documented in the same specimen.

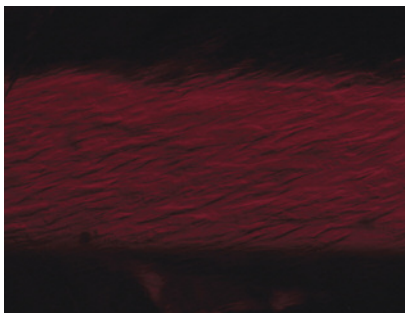

Figure 14. The zigzag-like growth structure observed in this 1.18 ct synthetic ruby is characteristic of hydrothermal growth. Field of view 1.42 mm.

Laser ablation–inductively coupled plasma–mass spectrometry (LA-ICP-MS) analysis revealed traces of Ca, Ti, Cr, Fe, Mo, Rh, Sn, W, and Pt. The low amount of Fe and Ti, the absence of V and Ga, and the presence of Pt were consistent with flux-grown corundum.

Both natural and flame-fusion synthetic ruby have been used as seed crystals in the flux growth of ruby (J.I. Koivula, "Induced fingerprints," Winter 1983 *G&G*, pp. 220–227; Summer 1991 Lab Notes, p. 112). The seed crystals are generally removed during the cutting process but may, on rare occasions, be detected in finished specimens. Upon close microscopic examination, we noted that several of the flux-filled healed fractures (wispy veils) extended into the areas showing hydrothermal graining. These observations led us to conclude that the hydrothermal material was a seed crystal and that the flux healing was a secondary process to the hydrothermal growth. There was an irregular separation between the materials under brightfield illumination.

This unusual combination of a hydrothermal ruby seed with flux ruby overgrowth is the first of its kind examined by GIA.

Ziyin Sun and Dino DeGhionno

Figure 15. When the synthetic ruby was examined under diffused fiber-optic lighting and darkfield illumination, hexagonal platinum platelets and trapped flux residue became apparent. Field of view 1.42 mm.

Rare Faceted WURTZITE

Recently the Carlsbad laboratory examined a 3.97 ct transparent brownish red pear-shaped modified brilliant for identification service (figure 16). Standard gemological testing revealed a refractive index that was over the limit of the RI liquid and a specific gravity (obtained hydrostatically) of 3.96. There was no fluorescence observed with exposure to long- and short-wave UV light. The stone also displayed an adamantine luster and a uniaxial optic figure when examined with polarized light. Microscopic examination with a fiber-optic light source showed fine needles and a large reflective decrepitation halo surrounding a negative crystal. Examination also revealed that the decrepitation halo was perpendicular to the optic-axis direction, suggesting the stone had basal cleavage (figure 17).

Figure 16. This 3.97 ct faceted wurtzite has an adamantine luster and brownish red bodycolor.

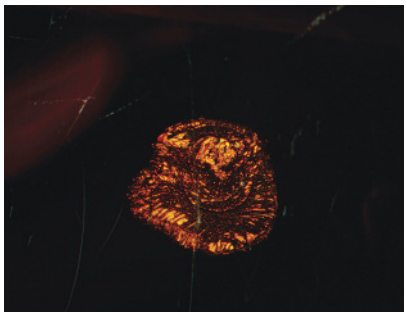

Figure 17. A decrepitation halo surrounds a negative crystal in the faceted wurtzite. Field of view 2.15 mm.

Raman spectroscopy and X-ray powder diffraction conclusively identified the stone as wurtzite. EDXRF analysis detected zinc and sulfur, which further supported this identification.

Wurtzite, a polymorph of sphalerite, commonly occurs in hydrothermal vein deposits associated with barite and sphalerite. Facet-grade wurtzite has been reported to occur in Merelani, Tanzania (Winter 2013 GNI, p. 261). This is the first wurtzite examined by the GIA laboratory.

Amy Cooper and Nathan Renfro

Tenebrescent ZIRCON

The Bangkok laboratory recently received for identification a 13.16 ct reddish orange stone, submitted as tenebrescent zircon (figure 18, left). Standard gemological testing indicated typical properties for the stable form of zircon: RI was over the detection limit of the standard refractometer, SG was approximately 4.50, and the sample was inert to both long- and short-wave UV. After exposure to short-wave UV for approximately 30 minutes, however, its tone became darker. Chemical analysis using EDXRF showed significant amounts of zirconium and silicon, as well as a trace amount of hafnium.

Tenebrescence, the phenomenon of reversible photochromism, is common in gemstones such as hackmanite (a variety of sodalite) but unusual in zircon. In September 2011, GIA examined two zircons from central Australia that

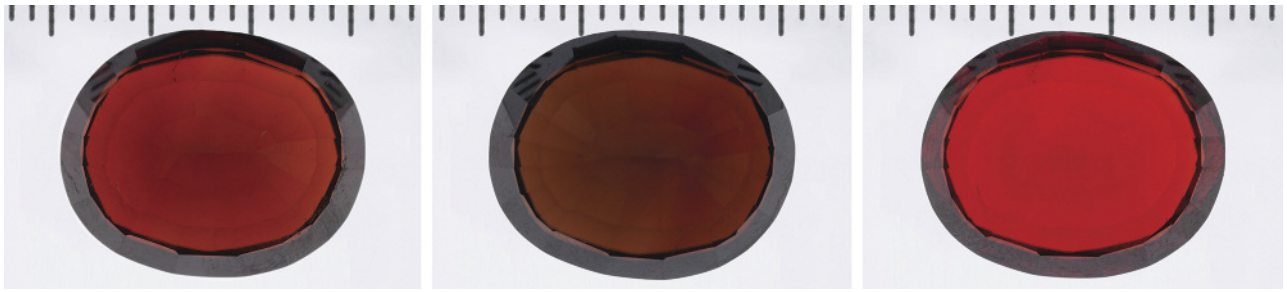

Figure 18. This 13.16 ct zircon is shown before (left) and just after 30 minutes of short-wave UV exposure (center). The SWUV lighting darkened the stone, while darkness restored the orange color. The image on the right shows the color of the stone after it was left in the dark for three weeks.

turned orange in darkness and faded to near colorless when exposed to light (S.F. McClure, "Tenebrescent zircon," Winter 2011 *G&G*, pp. 314–315). This zircon displayed a different phenomenon: Its reddish orange color did not fade under fluorescent lighting or fiber-optic light. Exposure to short-wave UV (SWUV) caused it to darken. The reddish orange component gradually diminished, and the stone appeared brown (figure 18, center). There was no further change after 30 minutes.

The UV-visible spectrum after SWUV exposure showed a significant increase in absorption in the 590–750 nm range, reducing transmission of the orange to red color and making the stone darker (figure 19).

As noted above, the reaction is reversible. The reddish orange color returned when the stone was stored in the dark at room temperature (see figure 18, right). The color change was obvious in the first 10 to 20 hours. After that, no further color change was observed.

To determine whether the process was repeatable, the stone was again subjected to SWUV. Once again the reddish orange color darkened in tone.

In summary, the reddish orange zircon was darkened by short-wave UV exposure, and the color returned when the stone was stored in the dark. The darkening reaction was much faster than the recovery. Further studies incorporating other conditions that might affect the rate of color modification in tenebrescent zircon are being conducted.

Ratima Suthiyuth

Figure 19. After 30 minutes of SWUV exposure, the zircon's absorption spectrum revealed more absorption in the 590–750 nm range, which relates to an orange to red color.

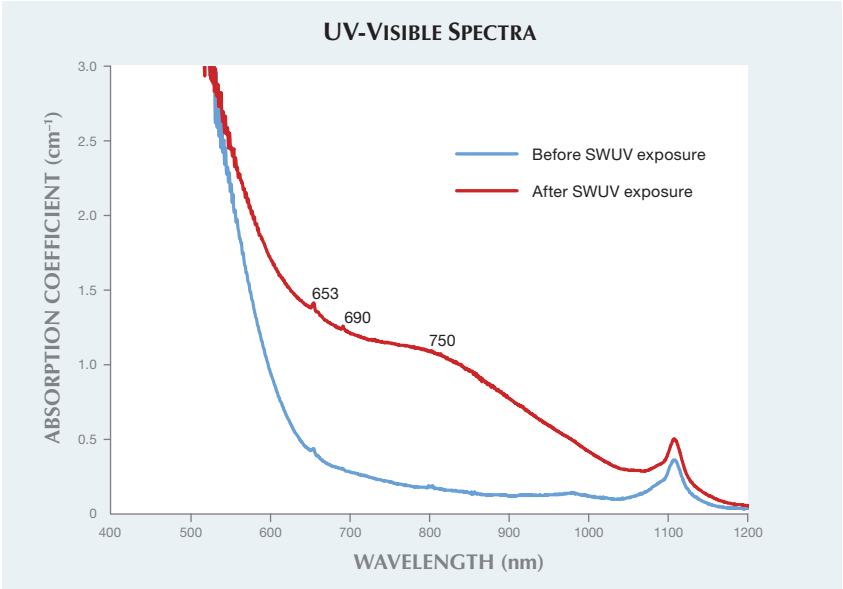

PHOTO CREDITS:
Robison McMurtry—1, 4; Troy Ardon—3; Lhapsin Nillapat—6; Charuwan Khowpong—7; Jian Xin (Jae) Liao—8; Chunhui Zhou—9, top; Jessie (Yixin) Zhou—9, bottom; Nathan Renfro—5, 14, 15, and 17; Sood Oil (Judy) Chia—11; Kyaw Soe Moe—13; Don Mengason—16; Sasithorn Engniwat—18.